www.sciencemag.org/cgi/content/full/1139038/DC1

Supporting Online Material for

Spin Rate of Asteroid (54509) 2000 PH5 Increasing Due to the YORP Effect

Patrick A. Taylor,* Jean-Luc Margot,* David Vokrouhlický, Daniel J. Scheeres, Petr Pravec, Stephen C. Lowry, Alan Fitzsimmons, Michael C. Nolan, Steven J. Ostro, Lance A. M. Benner, Jon D. Giorgini, Christopher Magri

*To whom correspondence should be addressed.
E-mail: ptaylor@astro.cornell.edu (P.A.T.); jlm@astro.cornell.edu (J.-L.M.)

Published 8 March 2007 on *Science* Express
DOI: 10.1126/science.1139038

This PDF file includes:

SUPPORTING ONLINE MATERIAL for Spin Rate of Asteroid (54509) 2000 PH5 Increasing due to the YORP Effect

Patrick A. Taylor,[1*] Jean-Luc Margot,[1*] David Vokrouhlický,[2]
Daniel J. Scheeres,[3] Petr Pravec,[4] Stephen C. Lowry,[5]
Alan Fitzsimmons,[5] Michael C. Nolan,[6] Steven J. Ostro,[7]
Lance A. M. Benner,[7] Jon D. Giorgini,[7] Christopher Magri[8]

[1]Department of Astronomy, Cornell University, Ithaca, NY 14853-6801, USA.
[2]Institute of Astronomy, Charles University, V Holešovičkách 2,
18000 Prague 8, Czech Republic.
[3]Department of Aerospace Engineering, University of Michigan,
1320 Beal Avenue, Ann Arbor, MI 48109-2140, USA.
[4]Astronomical Institute, Academy of Sciences of the Czech Republic,
Fričova 1, CZ-25165 Ondřejov, Czech Republic.
[5]School of Mathematics and Physics, Queen's University Belfast,
Belfast BT7 1NN, UK.
[6]Arecibo Observatory, HC3 Box 53995, Arecibo, PR 00612, USA.
[7]Jet Propulsion Laboratory, California Institute of Technology,
Pasadena, CA 91109-8099, USA.
[8]University of Maine at Farmington, 173 High Street - Preble Hall,
Farmington, ME 04938, USA.

*To whom correspondence should be addressed.
E-mail: ptaylor@astro.cornell.edu, jlm@astro.cornell.edu.

Methods

The shape modeling process produces a three dimensional model of the asteroid by minimizing the weighted squared residuals between the synthetic model and the one or two dimensional data sets. Three models of increasing complexity may be produced, typically in sequential order: (i) triaxial ellipsoid, described by the major axis length and axial ratios, (ii) harmonic, described by a spherical harmonic expansion of surface displacements, and (iii) vertex, described by a polygon with triangular facets. Shape modeling includes a degree of subjectivity in that one may, and typically must, introduce penalty functions to suppress shape features that mathematically reduce the residuals of the fit, but result in unphysical shapes (e.g., spiky surfaces or extreme concavities). Details on shape modeling and penalty functions can be found in (*S1*, *S2*).

For the (54509) 2000 PH5 shape models, we include 107 Doppler-only spectra from 2001 and 2004 for which the bandwidths were measured, 6 of the strongest Doppler-only spectra from 2005, 26 range-Doppler images (one rotation) from Goldstone in 2001, 228 range-Doppler images from Arecibo in 2004, and a well-sampled rotation from each of 20 optical lightcurves (*S3*). The pole, initial spin rate, and linear change in spin rate are as determined in the text. Radar scattering is modeled with with a cosine law of the form $R(C{+}1) \cdot cos^{2C}\theta$, where R is the Fresnel reflectivity at normal incidence, C is related to the near-surface structural complexity, and θ is the scattering angle (*S4*). Optical scattering is modeled with a Lambertian scattering law.

The same penalty functions that suppress unphysical shapes on large, medium, and small scales can also define the "roughness" of the surface on which the calculation of thermal torques is strongly dependent. On the largest scale, the accuracy of theoretical YORP accelerations depend on the overall size of the body (D^2 dependence) and the completeness of our knowledge of the surface. The lines of sight during the 2001 and 2004 radar observations of 2000 PH5 are

clustered within 20° of each other and ∼35° from the spin axis. Considering only regions of the surface within a 60° incidence angle of the radar, about 25% of the surface is either sampled at higher incidence angles or unsampled by the range-Doppler images. With a significant portion of one hemisphere unobserved, the smallest principal axis of inertia (the dimension parallel to the spin axis) is not well-constrained. We note that while photometric observations (*S3*) have more equatorial lines of sight, they cannot constrain this dimension because we treat them as relative photometry, which does not constrain the projected area responsible for producing the lightcurves.

During the ellipsoid model phase, the shape modeling software tends to produce disk-shaped models to decrease the weighted squared residuals. To probe different lengths of this axis, we invoke a flattening penalty that regulates how much the length along the spin axis can decrease. We find that in the final vertex model phase, disk-shaped models do not fit the data as well as less flattened models. On a medium scale, we can control the concavity of the surface to prevent the production of starfish-shaped bodies, typically during the spherical harmonic phase of shape modeling; vertex models tend not to require such a penalty. On the smallest scale, we can control the smoothness of the surface by penalizing shapes based on how non-coplanar adjacent facets are, thus suppressing serrated surfaces.

Table S1. Summary of the radar observations of 2000 PH5. The name column is the radar transmitting/receiving site: G for Goldstone and A for Arecibo. λ and β are the line of sight ecliptic longitude and latitude at the midpoint of the observations. Δ is the Earth-asteroid separation in AU. Type is Doppler-only spectra (D) or range-Doppler imaging (r-D). Resolutions are of the processed data. The start and stop times of the observations are in universal time. A run is a transmit-receive cycle. Goldstone images are coarser and have weaker signal to noise than the Arecibo images from 2004, but are an important consistency check on our shape and spin state. Arecibo images from 2005 are coarser than the Goldstone images providing only a few pixels on the target and are excluded from the shape modeling.

Name	Date	λ (deg)	β (deg)	Δ (AU)	Type	Resolution	Start-Stop (hhmmss)	Runs
G	27 July 2001	258	67	0.013	D	1.95 Hz	014144-020654	55
					r-D	18.75 m × 1.95 Hz	054416-074316	163
					r-D	18.75 m × 1.95 Hz	081641-093020	128
G	28 July 2001	275	55	0.016	r-D	37.5 m × 1.95 Hz	050210-053305	54
					D	1.95 Hz	055448-062657	61
					r-D	37.5 m × 1.95 Hz	063341-070343	51
A	27 July 2004	251	58	0.014	D	1 Hz	005342-005852	11
					r-D	15 m × 0.5 Hz	011305-013805	51
					r-D	7.5 m × 0.5 Hz	014000-014230	6
					r-D	15 m × 0.5 Hz	014347-020647	45
A	28 July 2004	267	49	0.017	D	1 Hz	014134-015314	21
					r-D	15 m × 0.5 Hz	015511-023053	64
					r-D	7.5 m × 0.5 Hz	023211-030753	62
					D	1 Hz	030916-031356	8
A	24 July 2005	192	16	0.037	D	2 Hz	201212-203942	23
					r-D	45 m × 1 Hz	204822-215414	53
					r-D	30 m × 1 Hz	215646-224106	36
A	25 July 2005	200	17	0.036	D	2 Hz	210206-212852	23
					r-D	45 m × 1 Hz	213158-230208	61
A	26 July 2005	207	18	0.036	D	2 Hz	212800-215415	22
					r-D	75 m × 1 Hz	221509-225933	37

Table S2. Radar reflection properties of 2000 PH5 in terms of circular polarization ratio μ (SC/OC, see Fig. S2), OC radar cross-section σ_{oc}, and OC radar albedo $\hat{\sigma}$ (*S5*, *S6*). Radar albedo is determined by dividing the radar cross-section by the average projected area of the 2000 PH5 shape model during the observations. The 10% and 25% uncertainties on μ and σ_{oc} are typical values based on variations in pointing accuracy and system parameters and are reasonable given the spread in the daily measurements. Radar-observed NEAs have μ roughly between 0 and 1 and $\hat{\sigma}$ roughly between 0 and 0.6 (*S5*).

Name	Date	μ	σ_{oc} (km^2)	$\hat{\sigma}$
G	27 July 2001	0.21	0.0016	0.13
G	28 July 2001	0.28	0.0010	0.08
A	27 July 2004	0.20	0.0017	0.14
A	28 July 2004	0.20	0.0023	0.19
A	24 July 2005	0.21	0.0013	0.13
A	25 July 2005	0.19	0.0014	0.13
A	26 July 2005	0.17	0.0012	0.12
	Average	0.21 ± 0.02	0.0015 ± 0.0004	0.13 ± 0.03

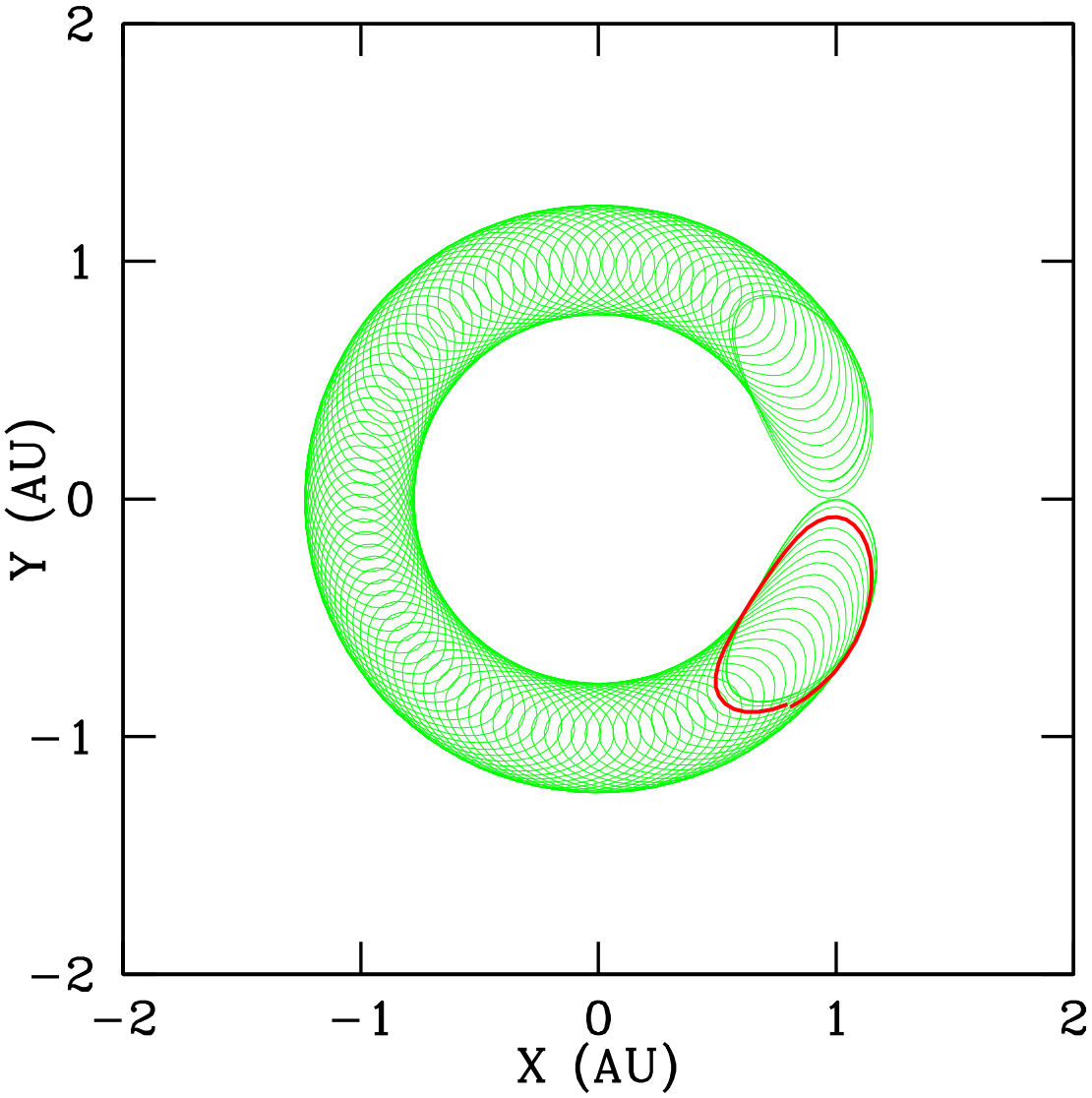

Fig. S1. Evolution of the position of 2000 PH5 in its Sun-Earth horseshoe orbit from 2003-2105 in a frame co-rotating with Earth. The 2007 trajectory is in red. The Sun is at the origin and Earth is at +1 on the x-axis. The trajectory of 2000 PH5 is a 1 year epicycle superimposed upon a roughly 100 year libration period between gravitational "bounces" off of Earth. Both the kidney-bean shape of the epicycle and the close Earth approaches occur because of the moderate eccentricity of 2000 PH5's orbit.

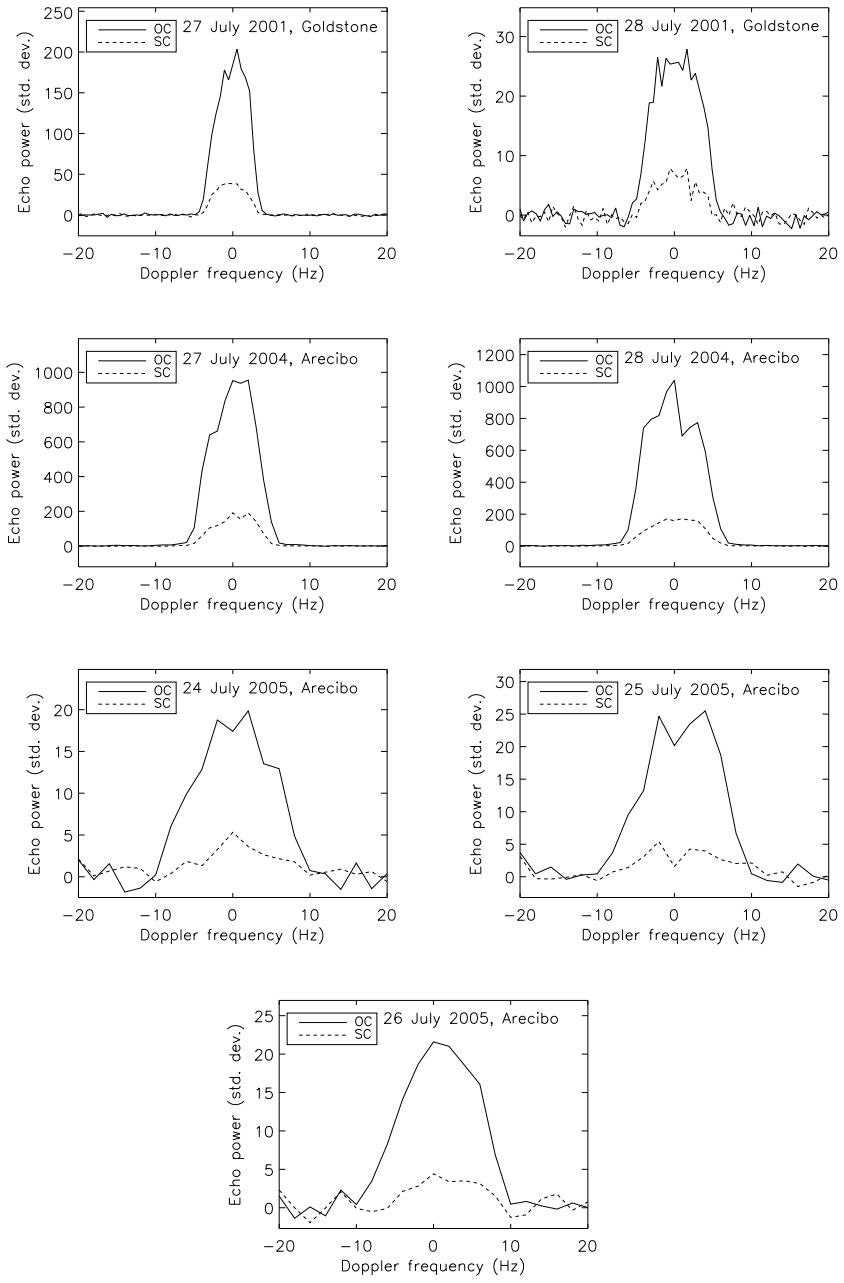

Fig. S2. Daily sums of Doppler-only spectra with echo power measured in standard deviations of the off-target noise. OC is the radar echo with the opposite circular polarization of the transmitted signal, and SC is the echo with the same circular polarization as the transmitted signal. Goldstone measurements are scaled to the Arecibo radar wavelength for easier comparison. The frequency resolution is then 0.54 Hz for the 2001 data, 1 Hz for the 2004 data, and 2 Hz for the 2005 data.

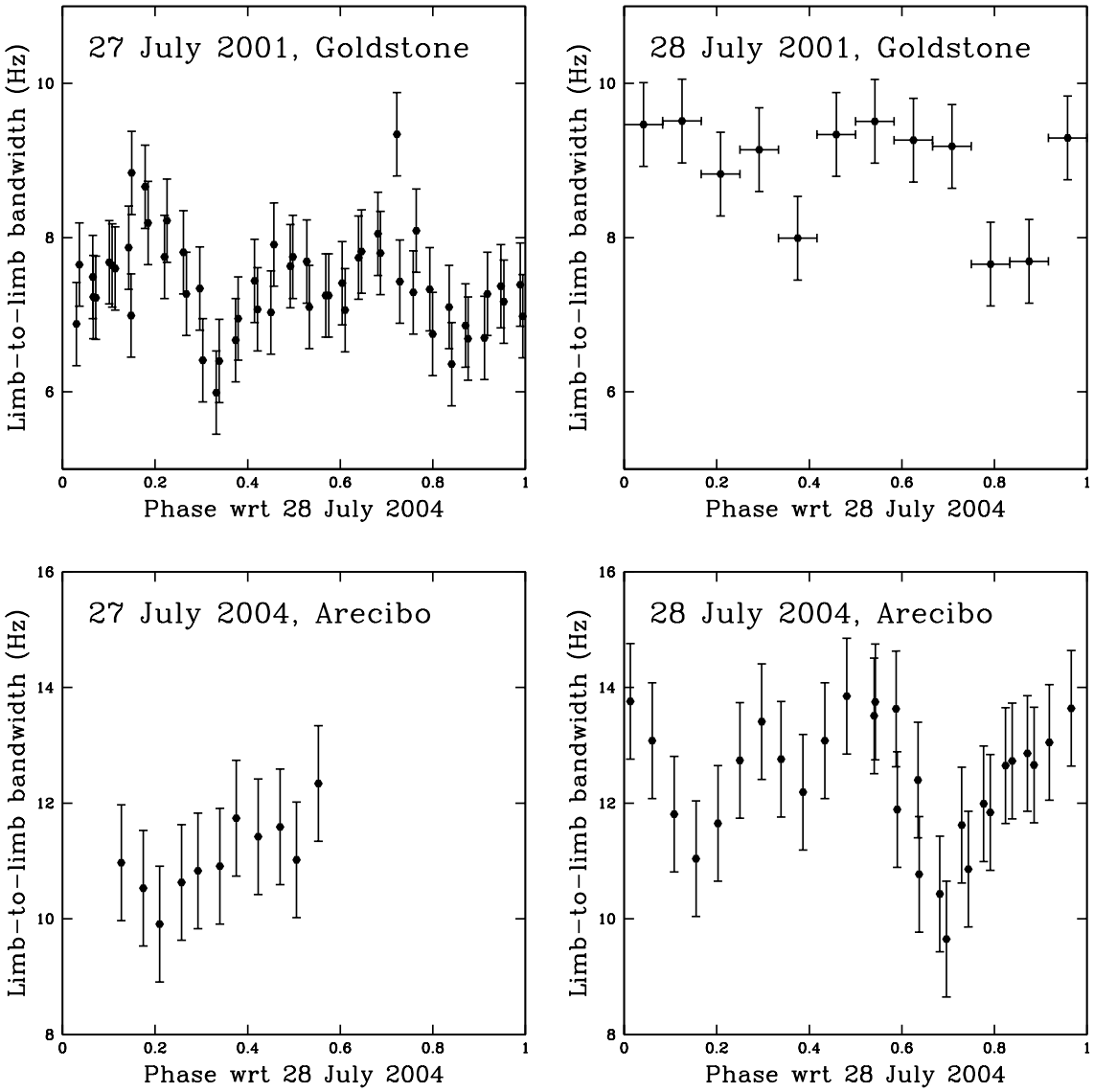

Fig. S3. Limb-to-limb radar bandwidth of 2000 PH5 observed in 2001 and 2004 as a function of rotation phase. Goldstone measurements are scaled to the Arecibo radar wavelength for easier comparison. Vertical error bars are the frequency resolution of the spectra (same as in Fig. S2). Bandwidths are measured for individual spectra for 27 July 2001, 27 July 2004, and 28 July 2004. The 28 July 2001 spectra are summed according to bins of 30° in rotation phase indicated by the horizontal error bars, while all spectra from each day of 24-26 July 2005 are summed to get a single bandwidth measurement. Overall, the mean bandwidth grows with time, increasing to approximately 19 Hz in July 2005, indicating the line of sight was moving away from the spin axis. The amplitude variation of the curves corresponds to the changing breadth of 2000 PH5 as it rotates.

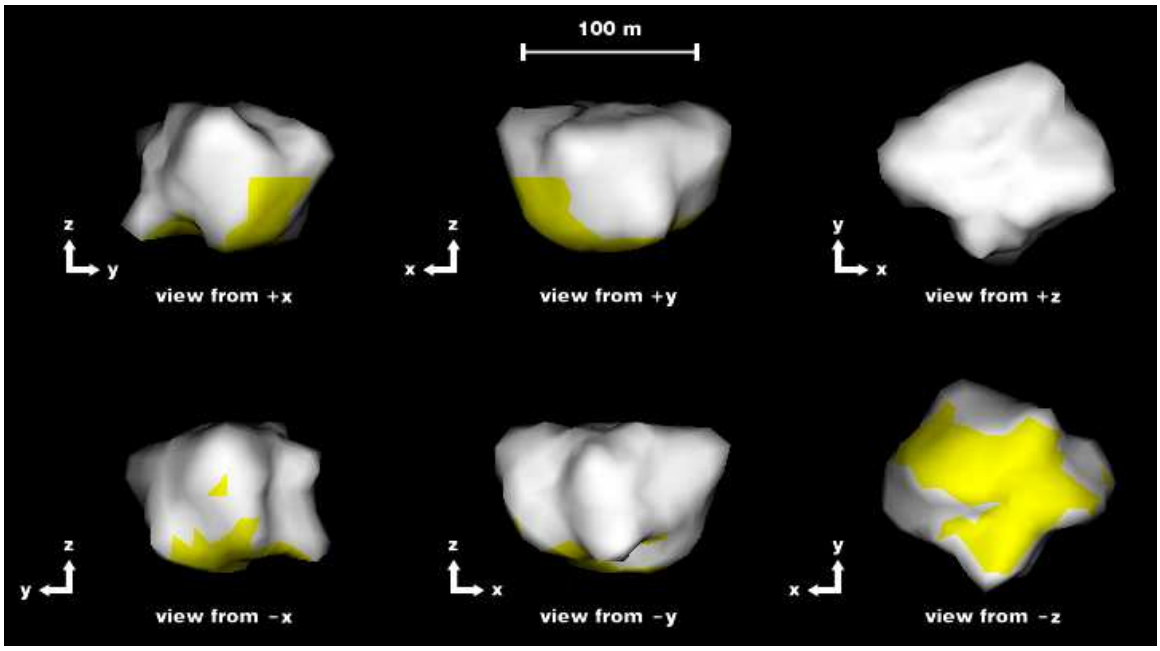

Fig. S4. Principal axis views of the best-fit 2000 PH5 vertex shape model. Yellow shading indicates the $\sim$25% of the surface that was effectively hidden from the view of the radar at incidence angles greater than 60°. The maximum extents along the principal axes x, y, and z are 149, 134, and 96 m, respectively. The northern hemisphere is flattened with clear linear edges in the top-right frame as well as a distinct concavity in the top-center and top-right frames.

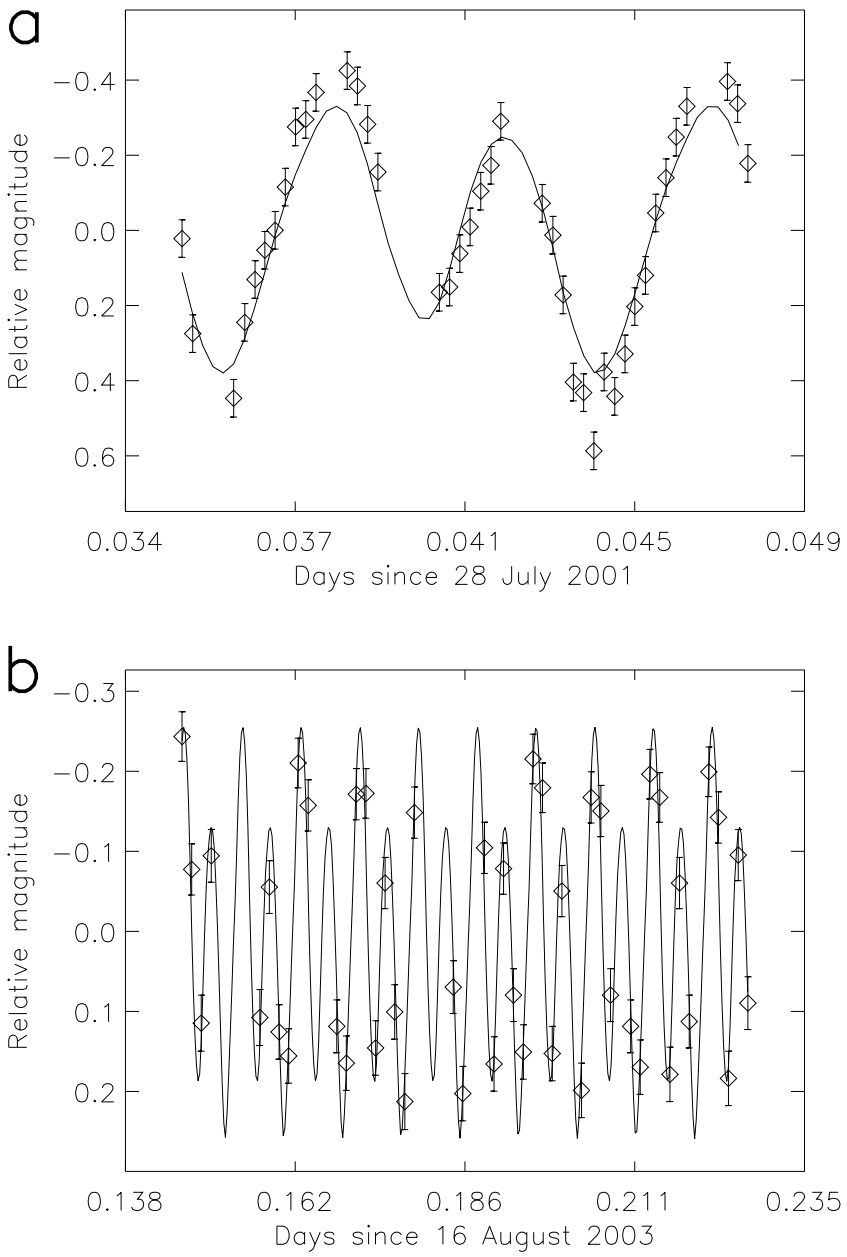

Fig. S5. Examples of synthetic lightcurves (solid lines) produced with the best-fit 2000 PH5 vertex shape model plotted with the observed lightcurves (♢) from 28 July 2001 and 16 August 2003. Including a linear change in sidereal spin rate allows for the synthetic and observed lightcurves to stay in phase over time. The maximum variation in amplitude of the synthetic lightcurves is ∼0.7 compared to the 1 magnitude variation observed in 2001 (a). In 2003 (b), the variations are comparable at 0.5 magnitudes.

References

S1. S. Hudson, *Remote Sensing Reviews* **8**, 195 (1993).

S2. C. Magri, *et al.*, *Icarus* **186**, 152 (2007).

S3. S. C. Lowry, *et al.*, *Science* (submitted).

S4. D. L. Mitchell, *Icarus* **124**, 113 (1996).

S5. S. J. Ostro, *Rev. Modern Phys.* **65**, 1235 (1993).

S6. S. J. Ostro, *et al.*, *Asteroids III*, W. F. Bottke, A. Cellino, P. Paolicchi, R. P. Binzel, eds. (Univ. of Arizona Press, 2002), pp. 151-168.